Structural and optical properties of 60B2O3–(20−x)Na2O–10PbO–10Al2O3:xTiO2:yNd2O3 glasses

ARTICLE *in* OPTICAL MATERIALS · OCTOBER 2013

Impact Factor: 1.98 · DOI: 10.1016/j.optmat.2013.07.021

Optical Materials 35 (2013) 2544–2550

Contents lists available at ScienceDirect

Optical Materials

journal homepage: www.elsevier.com/locate/optmat

Structural and optical properties of $60B_2O_3$–$(20-x)Na_2O$–$10PbO$–$10Al_2O_3$:$xTiO_2$:yNd_2O_3 glasses

N.C.A. de Souza [a], C.C. Santos [b], I. Guedes [c], N.O. Dantas [d], M.V.D. Vermelho [a,*]

[a] Instituto de Física, Universidade Federal de Alagoas, 57072-970 Maceió, AL, Brazil
[b] Departamento de Física, Universidade Federal do Maranhão, 65085-580 São Luís, MA, Brazil
[c] Departamento de Física, Universidade Federal do Ceará, Campus do PICI, Caixa Postal 6030, 60455-760 Fortaleza, CE, Brazil
[d] Laboratório de Novos Materiais Isolantes e Semicondutores (LNMIS), Instituto de Física, Universidade Federal de Uberlândia, 38400-902 Uberlândia, MG, Brazil

ARTICLE INFO

Article history:
Received 1 April 2013
Received in revised form 27 June 2013
Accepted 25 July 2013
Available online 30 August 2013

Keywords:
Borate glasses
Rare earth spectroscopy

ABSTRACT

In this work we investigate the effect of replacing Na_2O by TiO_2 on the structural and spectroscopic characteristics of the Nd_2O_3-doped $60B_2O_3$–$(20-x)Na_2O$–$10PbO$–$10Al_2O_3$:$xTiO_2$:yNd_2O_3 borate glass matrix. Measurements of X-ray patterns, glass temperatures (Tg), vibrational (Raman and infrared (IR)) and optical (absorption and emission) spectra were carried out. The trend of Tg, the Judd–Ofelt parameters and Nephelauxetic ratio as the TiO_2 and Nd_2O_3 concentration increases was interpreted quantitatively and qualitatively in terms of the network bonds and coordination numbers. Measurements of Tg across the Nd-doped glass series for different levels of Ti suggests changes in the rigidity of the matrix due to change of coordination of boron oxide resulting from the BO_4–BO_3 back conversion effect. The changes observed in the Raman and IR spectra are related to the $BO_3 \rightarrow BO_4$ conversion effect. The variation of the Judd–Ofelt parameters $\Omega_{(2)}$ and $\Omega_{(6)}$ indicates that the average rare earth-ligand radius decreases establishing an electronic density distribution when Nd^{3+} concentration increases. This effect is interpreted in terms of Judd–Ofelt parameters and by the bonding parameter $b^{1/2}$ due to Nephelauxetic effect.

1. Introduction

Borate glass systems have been shown promising properties to several technological applications, such as: thin amorphous films for battery application [1], bioactive glasses for tissue engineering [2] and nuclear waste disposals [2]. Concerning to photonics applications, borate glass properties are compatible to optical fiber development due to their low melting temperature and high rare earth loading capacity. The broadband luminescent emissions observed in rare earth doped glass matrices makes them excellent candidates to the development of tuneable or short pulse lasers [3], optical fiber amplifiers [4,5], and fiber lasers [6].

An increase on the luminescence bandwidth is essential to produce shorter laser pulses. However, this increase reduces the stimulated emission cross section which determines the laser gain and the rate of energy extraction [7]. The inhomogeneous broadening reflecting changes in the local rare earth environment increases the linewidth of the atomic transitions [8]. These changes in the multi component glass structures are essential to satisfy the requisites imposed on the possible glass applications. One example is the high rare earth doped glass pursued for compact lasers application [9–11].

Borate glasses have been extensively investigated as Nd_2O_3 host for lasers applications [7,12–18]. In particular, the use of transition metals oxides as network modifier is a constant in order to increase rare earth radiative parameters [12,19]. Recently, we investigated the structural changes in the B_2O_3–Na_2O–PbO–Al_2O_3–TiO_2 borate glasses when TiO_2 replaces for Na_2O. The optical absorption measurements indicated that the Urbach's energy reduced by 40% when TiO_2 content goes from 0 to 5 mol%, evidencing a possible change of the glass structure. The Raman data showed the following modifications: the appearance of a band ($\sim$850 cm^{-1}) related to the asymmetric vibration of "loose" BO_4^- tetrahedron, and the change in the intensity ratio of the bands at $\sim$772 cm^{-1} (assigned to the symmetric breathing vibration of six-membered rings with one BO_4 tetrahedron (triborate, tetraborate or pentaborate)) and at $\sim$797 cm^{-1} (assigned to the characteristic boroxol ring oxygen breathing vibration). This intensity change is related to the so-called BO_4–BO_3 back conversion, as verified from IR data. The BO_4–BO_3 back conversion effect accounts for the trend observed for Urbach's energy (E_U) and optical band gap (ΔE_{opt}). The overall results indicate that titanium (at least, up to 5 mol%) acts as a network modifier in the $60B_2O_3$–$(20-x)Na_2O$–$10PbO$–$10Al_2O_3$–$xTiO_2$ glasses.

This paper investigates the effects on such a structural variation due to the presence of rare earth ions. Structural and spectroscopic changes are analyzed by means of spectroscopic properties of rare

* Corresponding author. Tel.: +55 8232141439.
E-mail address: vermelho@fis.ufal.br (M.V.D. Vermelho).

0925-3467/$ - see front matter © 2013 Elsevier B.V. All rights reserved.
http://dx.doi.org/10.1016/j.optmat.2013.07.021

earth ions as well as for structural characteristics of the glassy matrix. Initially the changes in glass transition temperature, T_g, due to the increase in the Nd^{3+} concentration is analyzed in the light of the coordination number of these ions. Infrared spectroscopy, Raman and FT-IR, is also carried out to determine changes incurred in the matrix due to replacement of Na_2O by TiO_2. The investigation is concluded using optical spectroscopy, based on the Judd–Ofelt theory and Nephelauxetic effect, to infer the effects of the changes undergone in the glass from the point of spectroscopic characteristics of the rare earth ions.

2. Material and methods

The nominal composition of the glass system $60B_2O_3$–$(20-x)Na_2O$–$10PbO$–$10Al_2O_3$:$xTiO_2$:yNd_2O_3 is shown in the Table 1. Six batches containing different TiO_2 (0–5 mol%) and Na_2O (20–15 mol%) concentrations were doped with Nd_2O_3 in the range of 0–5.0 wt%. The 36 samples were prepared by the conventional melting–quenching method and the fabrication procedure is reported elsewhere [20].

The X-ray diffraction patterns were recorded using a XRD-6000 Shimadzu diffractometer with Cu Ka1 radiation (λ = 1.54056 Å). Differential Thermal Analysis (DTA) was performed by using a DTA-50 Shimadzu Differential Thermal Analyzer with the programmed heating rate at 20 °C/min.

The absorption measurements in the optical region 350–1000 nm were carried out using a LAMBDA 1050 UV/Vis/NIR spectrophotometer. Individual bands were measured in order to ensure the appropriated data accuracy to be used in the Judd–Ofelt and Nephelauxetic ratio calculations. The typical room-temperature ground-state Nd^{3+} absorption in the wavelength range from 400–900 nm are ascribed to $^4I_{9/2}$ ground state to the $^4F_{3/2}$, $^4F_{5/2}$ + $^4H_{9/2}$, $^4F_{7/2}$ + $^4S_{3/2}$, $^4F_{9/2}$, $^4H_{11/2}$, $^4G_{5/2}$ + $^4G_{7/2}$, $^4G_{7/2}$ + $^4G_{9/2}$, $^4G_{9/2}$ + $^4D_{3/2}$ + $^4G_{11/2}$, and $^4P_{1/2}$ + $^4D_{5/2}$ levels.

The luminescence measurements were carried out by means of a continuous wave (CW) Ti:Sapphire laser operating at 800 nm was focused down onto the sample by ×10 objective lens. The infrared fluorescence signals were collected perpendicularly to the laser beam by a lens telescope and dispersed by 9057 Sciencetech scanning spectrograph with spectral resolution <0.1 nm. The signals were detected by a Hamamatsu R406 photomultiplier tube for the visible–NIR portion of the spectra (400–1100 nm). A SR-530 Stanford Research lock-in amplifier coupled to a microcomputer was used for data acquisition and storage. The typical luminescent spectra have shown three bands at 890 nm, 1054 nm and 1330 nm characteristic of Neodymium ions in glass. There was no evidence of frequency upconversion effect.

For lifetime measurements we modulated the CW Ti:Sapphire laser beam at ~600 Hz by using a mechanical chopper located at the focus of a pair of 10 cm focal lens telescope. This frequency was chosen to provide the complete depopulation of the investigated rare-earth $^4F_{3/2}$ upper levels. The telescope provides a beam waist ~20 μm, ensuring the excitation cut-off time ~50 ns. The acquisition system time response consisting of photodetector and mechanical chopper was shorter than 1.0μs. The fluorescence signals were collected perpendicularly to the pump, filtered using a 10 nm bandwidth bandpass filter centered at 1064 nm, and acquired by a PDA10CF-EC – InGaAs Fixed Gain Detector (700–1800 nm, 150 MHz bandwidth). The lifetime signal data were recorded and stored in an oscilloscope before being downloaded to analysis. The relative errors in these measurements are estimated to be ±10%.

Table 1
Nominal composition of the glass system $60B_2O_3$–$(20-x)Na_2O$–$10PbO$–$10Al_2O_3$:-$xTiO_2$:yNd_2O_3 (BNPAxTyNd).

Code	Composition (mol%)					y Nd_2O_3 (wt%)
	B_2O_3	Na_2O	PbO	Al_2O_3	TiO_2	
BNPA0TyNd	60	20	10	10	0	y:0–5
BNPA1TyNd	60	19	10	10	1	y:0–5
BNPA2TyNd	60	18	10	10	2	y:0–5
BNPA3TyNd	60	17	10	10	3	y:0–5
BNPA4TyNd	60	16	10	10	4	y:0–5
BNPA5TyNd	60	15	10	10	5	y:0–5

The density of the glasses was measured by the Archimedes method using distilled water as the buoyancy liquid (ρ_w = 0.9971 at 25 °C) and a single pan balance, with an error of $\pm 10^{-5}$ g cm^{-3}. The concentration of Nd^{3+} ions (n) was found from the expression

$$n = 2\rho\frac{x}{100}\left(\frac{N_A}{P_M}\right)$$

where x is the rare earth doping level in wt%, ρ is the measured density, N_A is the Avogrado's Number, and P_M is the molecular weight.

The Raman spectra were recorded with a Jobin–Yvon T64000 triple-grating spectrometer using the 514.5 nm excitation line from an Ar^+ laser (Coherent Inc.,Innova70).The spectra were collected in back-scattering geometry with a resolution of 2 cm^{-1}. Detection of the Raman signal was carried out with a N_2-cooled CCD. The Fourier Transform Infrared (FT-IR) absorption spectra were recorded on a Bruker VERTEX70FT-IR spectrometer (resolution of 4 cm^{-1}), in the mid-region (400–4000 cm^{-1}), using the KBr pallet technique, and the signal was acquired using a DigiTect DLaTGS detector with an integrated preamplifier. The X-ray, optical absorption, Raman and IR measurements were recorded at room temperature.

3. Theory/calculation

The concept of "nephelauxetic effect" introduced by Jorgensen [21] is related to the shift of the absorption bands of transition metals and rare earth ions when they are in different environments as compared when they are in aqueous solutions. These shifts are interpreted in terms of ligand chemical bonds and provide an indirect but convincing evidence of metal–ligand orbital overlap. Owing to this effect, the molecular orbital becomes larger leading to the delocalization of the electron cloud over a larger area. As a consequence, the intermolecular repulsion in the host is weaker than that in the corresponding free ion suggesting a wider separation between the same orbital-electrons.

In other words, the reduction of the positive charge of the metal, which is transferred to the rare earth (RE^{3+}) ion, causes an increase in the covalence of the metal–ligand bond and the expansion of the f-shell increasing the effect of electrostatic repulsion. This overlap with the ligands reduces the value of the free-ion parameters and causes a contraction of the energy level structure of the ion in the glass. This contraction of the energy levels makes the wavelength of the absorption/emission bands shifts towards higher values. This change affects the spectroscopic properties of the rare earth elements, such as: covalence, polarizability, spin–orbit effect, coordination number for host, valence states of ions, bond anisotropy, as well as the overlap of wave functions.

The average nephelauxetic ratio ($\bar{\beta}$) is determined over the m transitions by

$$\bar{\beta} = \frac{1}{m}\sum\beta \tag{3.1}$$

where the individual nephelauxetic ratio, $\beta = v_c/v_a$, is determined by the ratio of the corresponding energies of respective transitions in the complex and aquo-ion environments.The overlap of the wavefunction relating a bonding parameter to the average nephelauxetic effect is obtained by considering that the f orbitals are

involved in the covalent bond formation with the ligand by the following metal wavefunction

$$\langle\Phi_{4f}| = (1-b)^{1/2}\langle 4f| - b^{1/2}\langle\Phi_{lig}| \tag{3.2}$$

where $b^{1/2}$ measures the amount of *4f*-ligand mixing. Thus, the average nephelauxetic ratio is related to the covalency factor by the relation

$$b^{1/2} = \left(\frac{1-\bar{\beta}}{2}\right)^{1/2} \tag{3.3}$$

A covalence parameter is defined by

$$\delta\% = \left(\frac{1-\bar{\beta}}{\bar{\beta}}\right) \times 100 \tag{3.4}$$

Thus, for β<1 and positive values of $\delta\%$ and $b^{1/2}$ the bonding in complex is more covalent in nature than that in the aqueous solution. The aqueous solution absorption bands for Nd^{3+} used in this calculation were determined by Carnall [22], where only absorption band maxima above 0.2 were considered.

The phenomenological parameters determined through the Judd–Ofelt theory also reflect changes in the environment containing the rare earth ion. They are determined by least square fitting of the measured electric-dipole oscillator strengths [23,24] to the relation:

$$f_{theo}(JJ') = \frac{8\pi^2 mcv}{3h(2J+1)e^2}\chi S_{ed}(JJ') \tag{3.5}$$

where $\chi = (n^2+2)^2/9n$ is the local field correction at the well-localized center in a medium of isotropic refractive index n and S_{ed} is the electric dipole line strengths given by:

$$S_{ed}(JJ') = e^2\sum\Omega_{(\lambda)}|\langle(SL)J|U^{\lambda}|(S'L')J'\rangle|^2 \tag{3.6}$$

The parameters calculations are performed minimizing the *rms* deviation of the measured and calculated oscillator strength $\delta_{rms} = \left(\sum_{i=1}^{p}(f_{meas}^{(i)} - f_{theor}^{(i)})^2/(p-3)\right)^{1/2}$ where p is the number of absorption bands used and 3 reflects the number of fitted parameters. These parameters are related to ligand field parameters through the relation [25]

$$\Omega_{(t)} = (2t+1)\sum_{p,s}|A_{s,p}|^2\Xi^2(s,t)(2s+1)^{-1} \tag{3.7}$$

The two main contributions to the $\Omega_{(t)}$ parameters arise from the $A_{s,p}$ and Ξ terms. The $A_{s,p}$ term is associated to the crystal field parameters of rank s and the pth component, being related to the structural changes in the vicinity of the rare earth ions. It is expressed by the following relation

$$A_{s,p} = (-1)^p\{(s-p)!/(s+p)!\}^{1/2}\sum_n g_n\frac{e^2}{r_n^{s+1}}P_s^p(\cos\phi_n) \times \exp(-ip\theta_n) \tag{3.8}$$

where g_n are ligand charges located at the position (r_n, ϕ_n, θ_n) in spherical coordinates with respect to the rare earth position. The rank s is determined by the triangular inequality for the angular moment coupling, $|1-t| \leqslant s \leqslant |1+t|$ (s = 1 or 3 for t = 2, s = 3 or 5 for t = 4, and s = 5 or 7 for t = 6) [26] .

The term Ξ is mainly affected by the covalence of the bonding between the rare earth and the surrounding atoms. Including the information related to the 3-*j* angular momentum symbols into $a(s,t)$ and $b(s,t)$ variables, it can be expressed by

$$\Xi(s,t) = \sum_n\left(a(s,t)\frac{\langle 4f|r|nd\rangle\langle nd|r^s|4f\rangle}{\Delta E(nd)} + b(s,t)\frac{\langle 4f|r|ng\rangle\langle ng|r^s|4f\rangle}{\Delta E(ng)}\right) \tag{3.9}$$

where $E()$ is the energy difference between the mixed $4f^N$ and $4f^{N-1}nl^1$ configurations, and the remaining terms account for the integrals of the one-electron wavefunctions.

The experimental procedure to determine the phenomenological parameters is described elsewhere [27,28]. The absorption bands were fitted using Gaussian spectral components to remove the linear background losses. It is also worth mentioning that whenever the overlap between two or more absorption bands exceeded 5% of their areas, their contributions to the determination of the phenomenological parameters of the Judd–Ofelt theory were considered as a single absorption band. This procedure was used for the $^4F_{5/2} + {}^2H_{9/2}$, $^4F_{7/2} + {}^4S_{3/2}$, $^4G_{5/2} + {}^2G_{7/2}$, $^4G_{7/2} + {}^2G_{9/2}$, $^4G_{9/2} + {}^2D_{3/2} + {}^4G_{11/2}$, and $^2P_{1/2} + {}^2D_{5/2}$ bands.

4. Results and discussions

Fig. 1 depicts the typical X-ray Diffraction (XRD) pattern of the BNPA0T0Nd and BNPA5T0Nd glasses. The two broad peaks at $2\theta = 27°$ and ~45°, as well as, the lack of crystalline structure evidence the random network picture of the glasses. No substantial changes are observed due to the incorporation of Nd_2O_3 into the glass matrices.

Fig. 2 displays the DTA spectrum for the BNPA0T0Nd and BNPA5T0Nd glasses. The glass transition temperature, T_g, as a function of Nd^{3+} content was investigated for two concentrations of TiO_2 (0 and 5.0 mol%) and the results are shown in the inset of

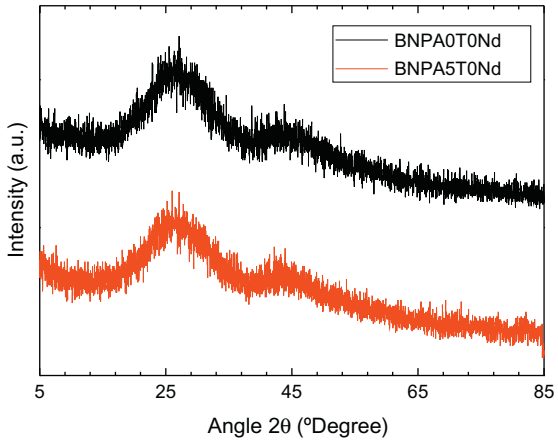

Fig. 1. X-ray diffraction pattern of the BNPA5T0Nd and BNPA5T0Nd glasses.

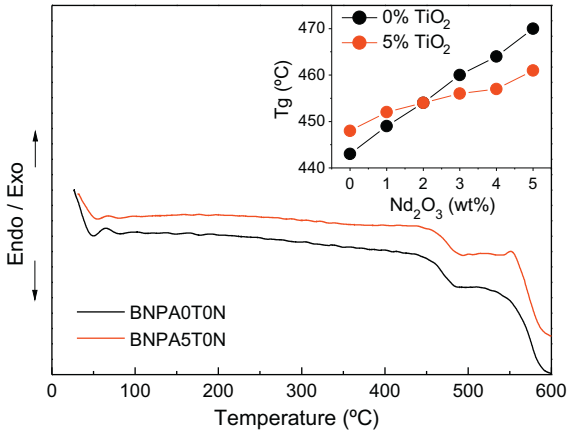

Fig. 2. DTA spectra of BNPA0T0Nd and BNPA5T0Nd glasses. The inset shows the variation of Tg as Nd^{3+} content increases for BNPA0T*y*Nd and BNPA5T*y*Nd.

the Fig. 2. We observe that T_g increases linearly with increasing the Nd^{3+} content for both BNPA0TyNd and BNPA5TyNd glasses. However the slope T_g/Nd^{3+} for the BNPA0TyNd (27/5) is steeper than that of BNPA5TyNd (13/5).

The observed increased in T_g is likely to be related to the formation of BO_4 and BO_3 groups. However, the high complexity to explain the nature of the transition temperature in glasses does not allow obtain conclusions about these results. Nevertheless, Kerner [29] and Tanaka [30] independently have developed models showing a strong correlation between variations in binary glasses transition temperature and the average coordination number of their components. They showed that the transition temperature increases as network modifier is added into binary glasses causing an increase in average coordination number. Stereometrical reasoning suggests a larger coordination number for larger ions [31]. Thus, the observed variation in T_g due to addition of Nd could be supported the mentioned models by considering the high coordination number required by the Nd ions (6–9). The fact that the more pronounced effect for the group of samples BNPA0TyNd than for samples BNPA5TyNd suggests that substitution of Na_2O by TiO_2 affects the Nd electronic density distribution reducing their coordination number. Further investigation is carried out using Judd–Ofelt analysis.

The typical room-temperature ground-state absorption spectra of Nd-free and Nd-doped glasses in the wavelength range from 300–1000 nm is shown in the Fig. 3. There is no visual evidence of change observed in the pure glass matrices owing to the substitution of Na_2O by TiO_2 is the reduction of the optical windows towards the infrared regions of the spectrum. The Nd-doped samples have shown the typical absorptions bands assigned as the $^4I_{9/2}$ ground state to the $^4F_{3/2}$, $^4F_{5/2} + {}^2H_{9/2}$, $^4F_{7/2} + {}^4S_{3/2}$, $^4F_{9/2}$, $^2H_{11/2}$, $^4G_{5/2} + {}^2G_{7/2}$, $^4G_{7/2} + {}^2G_{9/2}$, $^4G_{9/2} + {}^2D_{3/2} + {}^4G_{11/2}$, and $^2P_{1/2} + {}^2D_{5/2}$ levels and only subtle changes in the peaks position are observed.

The room-temperature luminescence spectra depicted in Fig. 4 show the typical emission bands at 890 nm, 1054 nm, and 1330 nm, ascribed to the $^4F_{3/2} \rightarrow {}^4I_{9/2}$, $^4F_{3/2} \rightarrow {}^4I_{11/2}$, $^4F_{3/2} \rightarrow {}^4I_{13/2}$ transitions, respectively. These luminescence spectra were normalized to the total area. The experimental apparatus' sensitivity does not allow the observation of substantial changes in their spectroscopic characteristics owing to the glass matrix changes, however, a small displacement is observed for highly TiO_2-doped samples.

The $^4F_{3/2} \rightarrow {}^4I_{11/2}$ lifetime reduced ~30% owing to concentration quenching effect, as depicted in the Fig. 5. Whilst the Na_2O–TiO_2 substitution, across a series of constant rare earth content, reduced the lifetime ~5%, evidencing glass matrices changes.

The change in the boron coordination can be probed by Raman and IR techniques. Fig. 6 displays the Raman spectra of BNPA0TyNd and BNPA5TyNd glasses. The assignment of the bands for BNPA0T0Nd was presented in Ref. [20]. Band #1 was assigned to chain-type metaborate groups (~755 cm^{-1}), band #2 was assigned to the symmetric breathing vibration of six-membered rings with one BO_4 tetrahedron (triborate, tetraborate or pentaborate) at ~772 cm^{-1}, and band #3 was assigned to the characteristic boroxol ring oxygen breathing vibration at 797 cm^{-1}. Incorporation of Nd^{3+} ions produces no modification in the Raman spectra. The appearance of the band #4 (~835 cm^{-1}) assigned to the asymmetric vibration of "loose" BO_4- tetrahedron in the Raman spectrum of BNPA5TyNd glass is only due to the presence of TiO_2 molecules.

The variation of the intensity ratio ($I_{\#2}/I_{\#3}$) observed in Ref. [20,21] when TiO_2 concentration increases (see BNPA0T0Nd and BNPA5T0Nd) was attributed the BO_4–BO_3 back conversion effect, since the addition of TiO_2 decreases the alkali (Na_2O) content. The decrease of the number of BO_4 groups with increasing TiO_2 content was verified from IR measurements.

Fig. 7 shows the IR spectra of BNPA0TyNd and BNPA5TyNd glasses. Bands #3 (790–1150 cm^{-1}) and #4 (1150–1600 cm^{-1}) correspond to the B–O stretching of the BO_4 and BO_3 groups, respectively.

The insets show the variation of the relative integrated intensity Ar = A_4/A_3 as a function of the Nd^{3+} content for BNPA0TyNd and BNPA5TyNd glasses. A_3 and A_4 are the integrated intensity of the BO_3 and BO_4 bands, respectively. The integrated intensity is

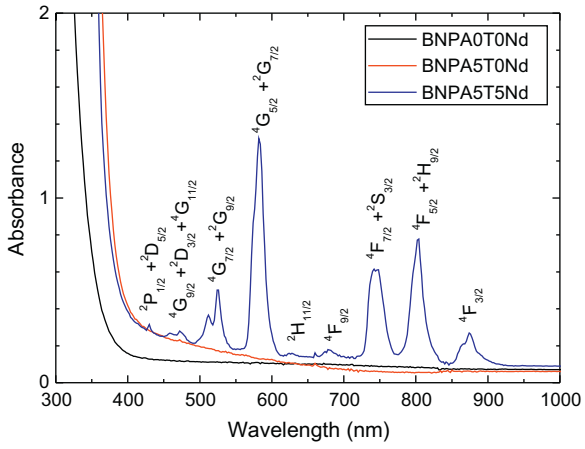

Fig. 3. Typical BNPA*x*TyNd absorption spectra for two different glass composition.

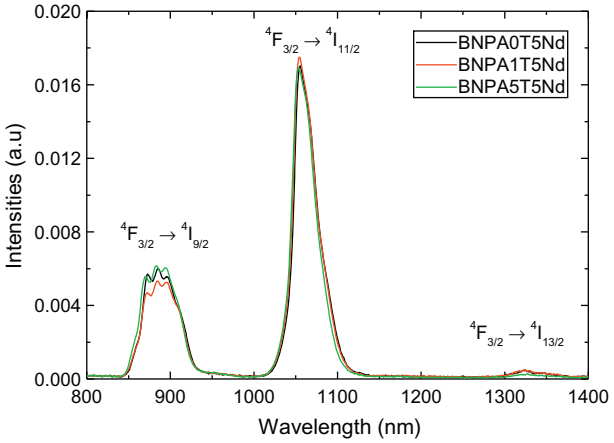

Fig. 4. Typical luminescence spectra for three different glass composition doped with 5 wt% of Nd^{3+}. All luminescent spectra are normalized $\int I(\lambda)d\lambda = 1$.

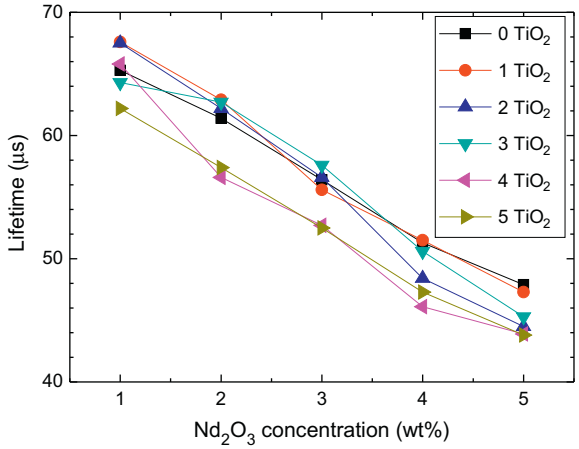

Fig. 5. Luminescence decay as a function of the rare earth concentration for different glass composition.

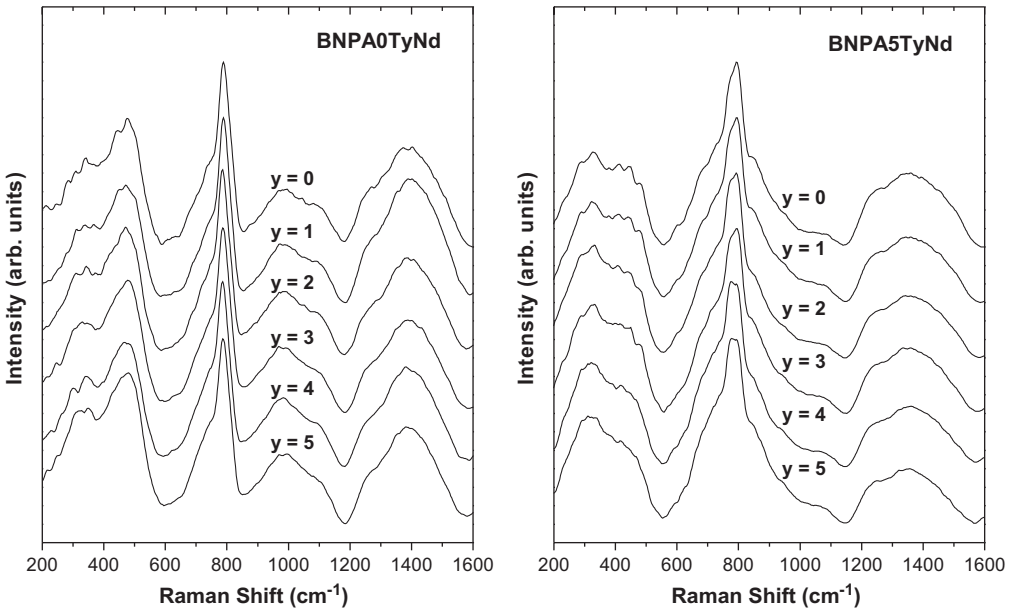

Fig. 6. The Raman spectrum of BNPA0T*y*Nd and BNPA5T*y*Nd glasses.

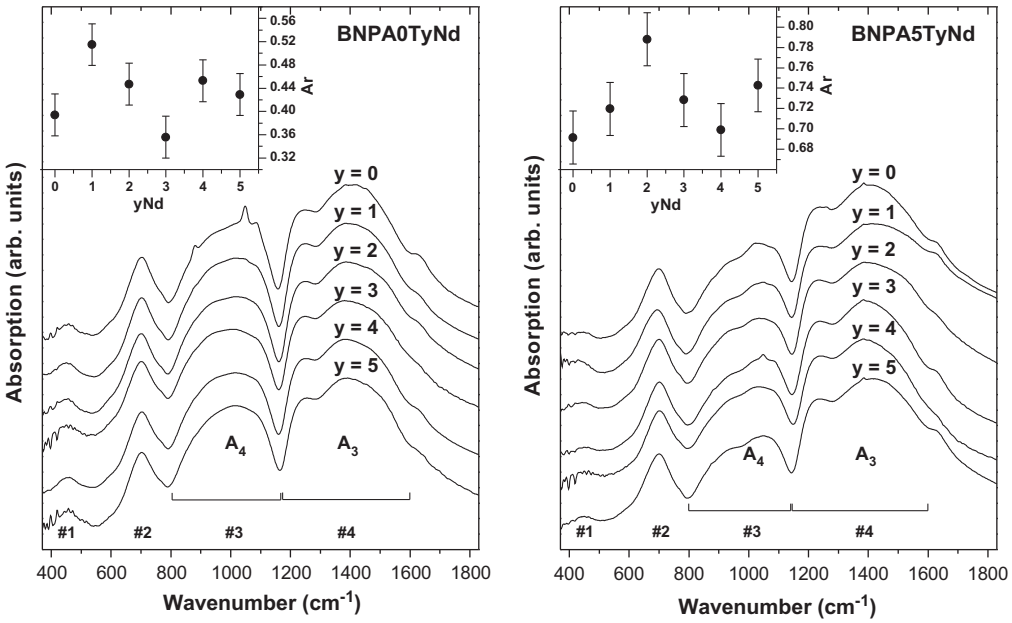

Fig. 7. The IR spectrum of BNPA0T*y*Nd and BNPA5T*y*Nd glasses.

calculated as the integral of the absorption signal using the software OPUS 6.5 available in the VERTEX 70FT-IR spectrometer. We observed that Ar for BNPA0T*y*Nd is smaller than that for BNPA5T*y*Nd, owing to the overall reduction of the BNPA5T*y*Nd integrated area A_4. As previously observed for Nd^{3+}-free $60B_2O_3$–$(20-x)Na_2O$–$10PbO$–$10Al_2O_3$:$xTiO_2$ glasses, incorporation of Ti^{4+} led to a $\sim$ 40% smooth reduction of the BO_4 groups due to the BO_4–BO_3 back conversion effect.

Although the inclusion of Nd_2O_3 into the glasses did not change considerably the values of Ar, it seems that Ar reaches a maximum ($\sim$0.79) for BNPA0T2Nd, which is shifted towards lower Nd_2O_3 concentration for BNPA5T1Nd. This suggests that there is interplay between Nd_2O_3 and TiO_2 oxides in the reduction of the BO_4 group. This interplay can also be observed in the data displayed in Table 2.

Table 2
Nominal Nd_2O_3 concentration in wt% and the respective amount of rare earth in ions/cm^3.

Nominal Nd concentration (wt%)	Nd concentration ($\times 10^{20}$ # cm^{-3})	
	0 mol% TiO_2	1–5 mol% TiO_2
1	0.7468	0.627 ± 0.007
2	1.5172	1.27 ± 0.03
3	2.2756	1.89 ± 0.03
4	3.0644	2.55 ± 0.05
5	3.8912	3.21 ± 0.05

For a given nominal concentration of Nd_2O_3, there is a reduction of the order of $\sim$15–18% due to the addition of 1 mol% of TiO_2.

However, these values slightly vary when the amount of TiO_2 increases from 1 to 5 mol%.

The effect of replacing Na_2O for TiO_2 into the BNPA*x*T*y*Nd glasses can also be probed by analysing the Judd–Ofelt parameters, which allows one to analyze the changes in the glass environment under the spectroscopic point of view of the rare earth interactions according Eq. (3.8). We observe that the values of $\Omega_{(2)}$ for BNPA5-T*y*Nd are greater than those for BNPA0T*y*Nd as depicted in the Fig. 8(a). The increasing in the $\Omega_{(2)}$ value is a consequence of the reduction of the average rare earth-ligands radial distribution $r^{-(s+1)}$ due to the addition of TiO_2, as can be inferred from Eq. (3.8), due to the spatial distribution implicit in the parameter $A_{s,p}$. It is imposed by the triangular inequality for the angular moment coupling defining the rank s (=1 or 3) for $t = 2$ as the major contribution to $A_{s,p}$. Additionally, despite the measurement accuracy difference for each method, it is evident the similarities between the behavior of $\Omega_{(2)}$ and the ratio between the spectra of BO_4 and BO_3 (Ar). This suggests that the change undergone in the environment due to BO_4–BO_3 back conversion effect likewise affects the Nd ions ligands environment. As a result, the substitution of Na_2O by TiO_2 brings about a more compact glass structure. Fig. 8(b) shows that $\Omega_{(6)}$ parameters have also shown variation with similar trend due to the BO_4–BO_3 back conversion effect. However, their analysis, and the $\Omega_{(2)}$ parameter, will be carried out considering the simultaneous substitution of Na_2O by TiO_2, as well as the addition of Nd_2O_3.

Fig. 9(a) depicts the overall changes undergone in the $\Omega_{(2)}$ parameter. The results show reduction on the $\Omega_{(2)}$ value due to the augment of Nd_2O_3 content. However, it is also noticed that across the different Nd contend series, the Na_2O by TiO_2 substitution increases the $\Omega_{(2)}$ parameter values. It becomes evident the saturation like trend on the $\Omega_{(2)}$ dependent on TiO_2 concentration. The 1.0 wt% Nd-doped samples exhibit saturation onset at TiO_2 around 1.0 mol%. The saturation onsets shift towards the higher TiO_2 concentration for higher the Nd_2O_3 concentrations. This suggests that, at lower rare earth concentration (~1.0 wt%), only the initial environmental change caused by presence of TiO_2 affected the rare earth ions chemical bonds and consequently their coordination number.

A qualitatively analyzed can be addressed based on the chemical bond polarity of the Nd_2O_3, Na_2O and TiO_2 compounds, and their respective electronegativity to characterize their bond nature character. The TiO_2 is considered a covalent polar, or a covalent with partial ionic character, (with the difference in the electronegativity $\Delta = 1.90$), while Nd_2O_3 ($\Delta = 2.30$) and Na_2O ($\Delta = 2.51$) are ionic bond character in nature. Thus, the substitution of Na_2O by

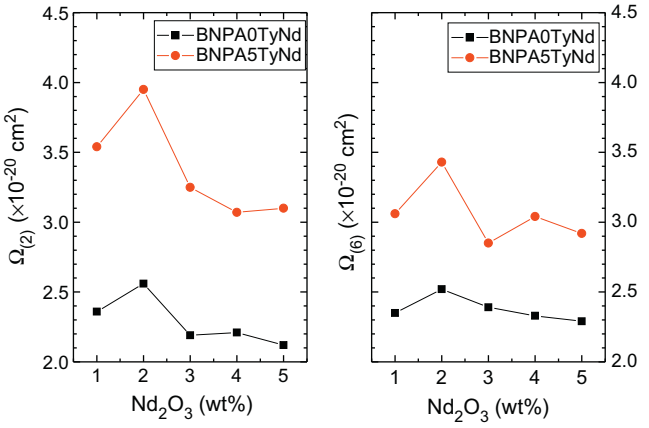

Fig. 8. $\Omega_{(2)}$ and $\Omega_{(6)}$ Judd–Ofelt phenomenological parameters variation determined as function of the Nd content.

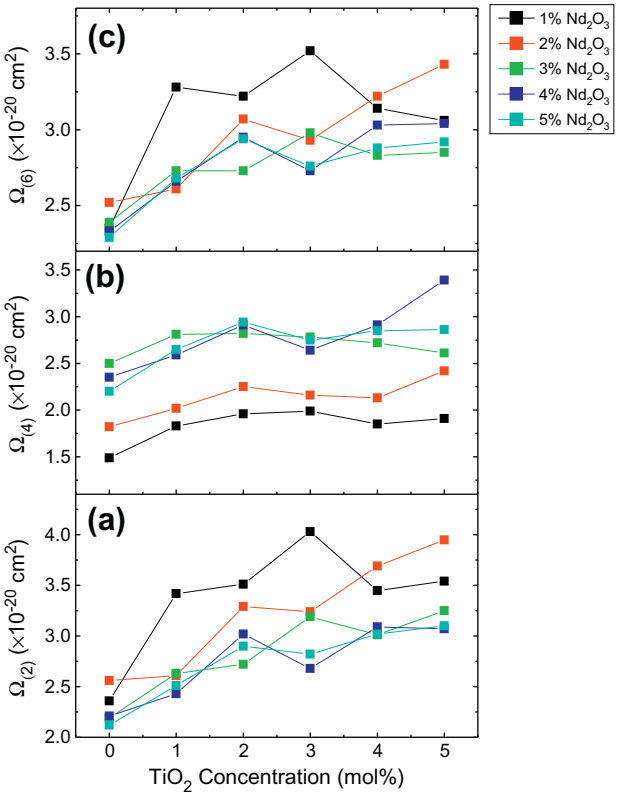

Fig. 9. (a) $\Omega_{(2)}$, (b) $\Omega_{(4)}$, and (c) $\Omega_{(6)}$ Judd–Ofelt phenomenological parameters.

TiO_2 allows changes in the charge density distribution inside the matrix affecting the Nd ions. The restriction of the localized density of charge required by the Na^+–O^{2-} ionic bonding is partially released due to the covalent character of Ti^{4+}–O^{2-}, moreover the coordination number of TiO_2 is higher than the Na_2O. The Ti covalent character bonds tend to share the oxygen charge density affecting their ionic character bond with neighbor Nd, provoking a density of charge redistribution causing an overall increasing on the $\Omega_{(6)}$ parameter values. This assumption is corroborated by Tanabe et al. [32] studying the contributions of the $\Omega_{(6)}$ intensity parameters of Er^{3+} ions in oxide glasses on ^{151}Eu Mössbauer spectra. They inferred that $\Omega_{(6)}$ is strongly affected by changes in the covalence owing to the radial integrals $\langle 4f|r^s|nl\rangle$ contribution. They observed decrease of the $\Omega_{(6)}$ parameter as a result of increasing of the 6*s* electron density; attributed to the overlapping integrals of the 4*f* and 5*d* affected via the shield effect of the 6*s* orbital. Fig. 9(c) shows that the changes on the rare earth electronic configuration environment due to the substitution of Na_2O–TiO_2 reach stability according to the Nd_2O_3 contend. Further addition of titanium oxide does not affect the $\Omega_{(6)}$ intensity. Furthermore, it is also noticeable that the value of $\Omega_{(6)}$ reduces for larger amount of rare earth. The high rare earth contends enables the clustering formation, and, owing to the Nd_2O_3 ionic bond characteristics increases the Nd^{3+} 6*s* electron density reducing the $\Omega_{(6)}$ value. On the other hand, rare earth clustering formations tend to increase their coordination number.

As the clustering formation is unlike to occur at low rare earth concentration, the saturation like effect suggests that a density of charge equilibrium was achieved. Thus, the saturation onset shifting towards the higher TiO_2 concentration for highly Nd-doped samples may be attributed to the clustering formation and an increase in their coordination number. The suggested change in the coordination number is consistent with the trend of the T_g shown in the Fig. 2. The two sets of samples BNPA0T*y*Nd and BNPA5T*y*Nd

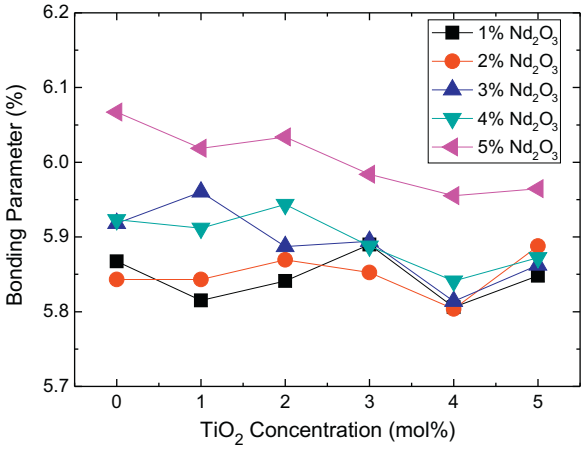

Fig. 10. Bonding parameters ($b^{1/2}$) variation across the series of different Nd_2O_3 concentration as a function of TiO_2 contends.

are under the effect of formation of agglomerates. However, BNPA5T*y*Nd require lower coordination number due to the reduction in distribution of charge density on layer 6*s* of Nd ions. This effect causes the slope reduction.

The analysis applied for $\Omega_{(6)}$ corroborates the behavior for the observed $\Omega_{(2)}$. The Nd clustering formation tends to increases the average rare earth-ligands radial distance. This reflects in reduction of the values of $\Omega_{(2)}$ parameters for high Nd concentrations. Moreover, the glasses become more compact due to the BO_4 to BO_3 back conversion caused by the sodium–titanium substitution. This fact tends to reduce the average radial distance enhancing the $\Omega_{(2)}$ value. The relation between the Ar and $\Omega_{(2)}$ similarity are depicted in the Figs. 7 and 9, respectively.

The assumptions of change in covalency proposed to explain the $\Omega_{(6)}$ trends is corroborated following the bonding parameter variation, $b^{1/2}$, determined through the Nephelauxetic ratio. As depicted in the Fig. 10, it is evident the enhancement in the $b^{1/2}$ value due to the increasing in the rare earth concentration. It is also noticeable that for one specific Nd_2O_3 concentration the addition of TiO_2 reflects in reductions in the parameter value. According to Eq. (3.4), an increasing in $b^{1/2}$ reflects reductions on the average Nephelauxectic. This reduction is a consequence of the contraction of the energy level structure in the glass due to electrostatic repulsion caused by an excess of charge in the 4*f*-shell. This is in agreement with the assumption of the increase in the Nd 6*s* electronic density of charge which resulted in decrease of $\Omega_{(6)}$. Consequently, a reduction in the $b^{1/2}$ parameter represent an increase in the 6*s* charge density.

5. Conclusions

In this work the effect of TiO_2 replacing Na_2O on lead borate glasses was investigated. Qualitative chemical bond polarity analysis due to the replacement of Na_2O by TiO_2, as well as stereometric reasoning, suggested glass modifications that, from the viewpoint of the network former ions, caused reductions on the Boron coordination number which led to the BO_4 to BO_3 back conversion effect. From the point of view network modifiers, the Judd Ofelt theory and Nephelauxectic effect allowed analysis which shown changes on the electronic density of charge of the Nd ions. The charge density redistribution caused by the polar covalent character bond of the TiO_2 when replacing the Na_2O bonds led to an increasing on the Nd–O covalency, reducing their coordination number. On the other hand, high rare earth concentrations favored rare earth clustering formation. This effect reduces the Nd–O covalency, due to the ionic character of Nd, in contrast with the effect of the Na_2O–TiO_2 substitution increasing their coordination numbers. The increased coordination number has led to changes in the glass characteristics which increased the glass transition temperature (T_g) of the matrix. The effect T_g variation was less pronounced in glasses containing higher titanium concentrations. This showed consistence with the reduction on the Nd electron density caused by the replacement of Na_2O by TiO_2.

Acknowledgments

The financial support for this research by FINEP, CNPq, CAPES, Brazilian Agencies, are gratefully acknowledged. One of the authors N.C.A.S. is supported by graduate studentship from CNPq.

References

[1] K. Cho, J. Oh, T. Lee, D. Shin, Journal of Power Sources 183 (2008) 431–435.
[2] S. Baccaro, N. Catallo, A. Cemmi, G. Sharma, Nuclear Instruments & Methods in Physics Research Section B-Beam Interactions with Materials and Atoms 269 (2011) 167–173.
[3] Y.J. Chen, X.H. Gong, Y.F. Lin, Z.D. Luo, Y.D. Huang, Optical Materials 33 (2010) 71–74.
[4] K. Kuroda, K. Sasahira, Y. Yoshikuni, Optical Fiber Technology 18 (2012) 44–46.
[5] G. Sobon, P. Kaczmarek, K.M. Abramski, Optics Communications 285 (2012) 1929–1933.
[6] H. Djellout, R. Mokdad, M. Benarab, F.A. Ouamer, M. Tamine, O. Lamrous, P. Meyrueis, Optical Engineering 51 (2012).
[7] K.S.R. Koteswara Rao, M.B. Saisudha, H.L. Bhat, J. Ramakrishna, Journal of Applied Physics 9 (1996) 4845–4853.
[8] J.R. Bonar, M.V.D. Vermelho, P.V.S. Marques, A.J. McLaughlin, J.S. Aitchison, Optics Communications 149 (1998) 27–32.
[9] R. Mary, S.J. Beecher, G. Brown, R.R. Thomson, D. Jaque, S. Ohara, A.K. Kar, Optics Letters 37 (2012) 1691–1693.
[10] C. Horvath, A. Braun, H. Liu, T. Juhasz, G. Mourou, Optics Letters 22 (1997) 1790–1792.
[11] M.V.D. Vermelho, U. Peschel, J.S. Aitchison, Journal of Lightwave Technology 18 (2000) 401–408.
[12] M.B.S.A.J. Ramakrishna, Physical Review B 53 (1995) 6186–6196.
[13] A.V.P.O.B. Petrova, V.E. Shukshin, K. Voron'ko, J. Opl. Technol 78 (2011) 659–663.
[14] J. Pisarska et al., Journal of Alloys and Compounds 451 (2007) 223–225.
[15] L.C. Courrol et al., Journal Luminescence 102–103 (2003) 101–105.
[16] B. Karthikeyan, S. Mohan, Physica B 334 (2003) 298–302.
[17] K.S.T. Shaweta Mohan, Gopi Sharma, Leif Gerward, Spectrochimica Acta Part A 70 (2007) 1173–1179.
[18] Lilia C. Courrol, Luciana Reyes P. Kassab, Vanessa D. Del Cacho, Sônia H. Tatumi, Laércio Gomes, Niklaus U. Wetter, Journal of Non-Crystalline Solids 384 (2004) 98–102.
[19] J. Pisarska et al., Journal of Molecular Structure (2006) 201–206.
[20] N.C.A. de Sousa, M.T. de Araujo, C. Jacinto, M.V.D. Vermelho, N.O. Dantas, C.C. Santos, I. Guedes, Journal of Solid State Chemistry 184 (2011) 3062–3065.
[21] C.K. Jørgensen, North-Holland Pub. Co., Amsterdam, 1971.
[22] P.R.F.W.T. Carnall, K. Rajnak, Journal of Chemical Physics 49 (1968) 4424.
[23] B.R. Judd, Physical Review 127 (1962) 750.
[24] G.S. Ofelt, Journal of Chemical Physics 37 (1962) 511.
[25] W.F. Krupke, Physical Review 145 (1966) 325.
[26] R.C. Powell, Physics of Solid-State Laser Materials, AIP Press/Springer, New York, 1998.
[27] C.C. Santos, I. Guedes, C.K. Loong, L.A. Boatner, A.L. Moura, M.T. de Araujo, C. Jacinto, M.V.D. Vermelho, Journal of Physics D-Applied Physics 43 (2010).
[28] T.B. Brito, M.V.D. Vermelho, E.A. Gouveia, M.T. de Araujo, I. Guedes, C.K. Loong, L.A. Boatner, Journal of Applied Physics 102 (2007).
[29] R. Kerner, M. Micoulaut, Journal of Molecular Liquids 71 (1997) 175–186.
[30] J.G.E.K. Pátek, London, 1970.
[31] K. Tanaka, Solid State Commun 54 (1985) 867–869.
[32] S. Tanabe, T. Ohyagi, S. Todoroki, T. Hanada, N. Soga, Journal of Applied Physics 73 (1993) 8451–8454.